

Covalent Organic Frameworks with Record Pore Apertures

Zhenjie Mu, Yuhao Zhu, Bixiao Li, Anwang Dong, Bo Wang, and Xiao Feng*



Cite This: *J. Am. Chem. Soc.* 2022, 144, 5145–5154



Read Online

ACCESS |



Metrics & More

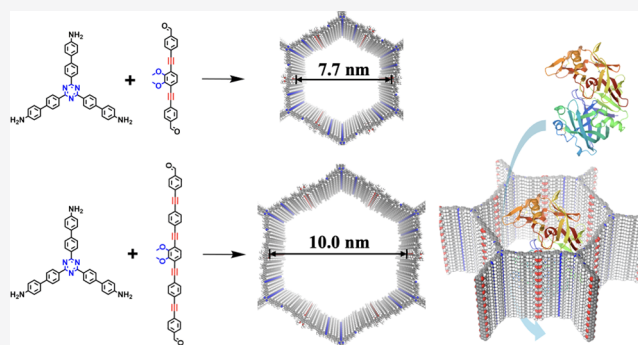


Article Recommendations



Supporting Information

ABSTRACT: The pore apertures dictate the guest accessibilities of the pores, imparting diverse functions to porous materials. It is highly desired to construct crystalline porous polymers with predesignable and uniform mesopores that can allow large organic, inorganic, and biological molecules to enter. However, due to the ease of the formation of interpenetrated and/or fragile structures, the largest pore aperture reported in the metal–organic frameworks (MOFs) is 8.5 nm, and the value for covalent organic frameworks (COFs) is only 5.8 nm. Herein, we construct a series of COFs with record pore aperture values from 7.7 to 10.0 nm by designing building blocks with large conformational rigidness, planarity, and suitable local polarity. All of the obtained COFs possess eclipsed stacking structures, high crystallinity, permanent porosity, and high stability. As a proof of concept, we successfully employed these COFs to separate pepsin that is ~ 7 nm in size from its crudes and to protect tyrosinase from heat-induced deactivation.



INTRODUCTION

In the pursuit of diverse functions and good control of porous structure with atomic precision, crystalline porous materials, such as metal–organic frameworks (MOFs)^{1,2} and covalent organic frameworks (COFs), have been explosively developed in recent decades.³ The physical and chemical features of the pores in these materials determine the kinds of the substances that can enter into, interact with, and pass through, where the pore apertures mainly dominate the size and shape selectivity.^{4,5}

Particularly, COFs are constructed by organic building blocks via covalent bonding, featuring tailorable and long-range ordered skeletons with high crystallinity and porosity.^{3,6–14} They possess well-defined and easily tuned pore channels that allow the mass transfer of target molecules with different polarities and dimensions, endowing the COFs with great potentials in gas storage and separation,^{15–19} heterogeneous catalysis,^{20–28} optoelectronics,^{29–31} energy storage and conversion,^{32–43} sensing,^{44–46} etc.^{47–51} The pore apertures of COFs dictate the size of target molecules that can permeate into the pores, which provide active sites and/or confined space to perform corresponding functions.⁵² For the applications requiring the inclusion and/or separation of large organic, inorganic, and biomolecules, it is highly desired to construct COFs with suitable large pores. To the best of our knowledge, Fang et al. reported JUC-564 that has the largest pore (4.3 nm) in three-dimensional COFs.⁵³ Li et al. and Liu et al. reported that both Ttba-TPDA-COF and PC-COF, respectively, have the largest pores (5.8 nm) in two-dimensional (2D) COFs.^{54–56} Yaghi et al. prepared MOF-

74-XI, which exhibited the largest MOF pore aperture with an opposite edge-to-edge distance of 8.5 nm.⁵² In principle, long linkers can be used to obtain crystalline polymers with larger pore apertures. However, attempts to construct large-pore COFs often yield interpenetrated amorphous structures with smaller pores.^{3,9,57,58}

As reported in the literature, increasing the conformational rigidness and planarity of the monomers is important for obtaining crystalline 2D COFs. Herein, we proposed a strategy to construct COFs with large mesopore apertures via minimizing the interlayer nonbond energy by further introducing appropriate polarity of the building blocks. We prepared a series of COFs (TDCOF-1, TDCOF-2, and TDCOF-3) with the opposite edge-to-edge distances ranging from 7.7 to 10.0 nm in the hexagonal cross section. The diagonal length of the pore apertures in TDCOF-3 can reach up to 11.5 nm. To the best of our knowledge, these COFs possess the largest pore apertures among the reported MOFs and COFs synthesized via bottom-up methods. All three COFs exhibit robust backbones, as demonstrated by their high crystallinity, permanent porosity, and high thermal and hydrostability. We utilized these TDCOFs as column-packing materials to successfully separate pepsin from its raw materials.

Received: January 17, 2022

Published: March 8, 2022



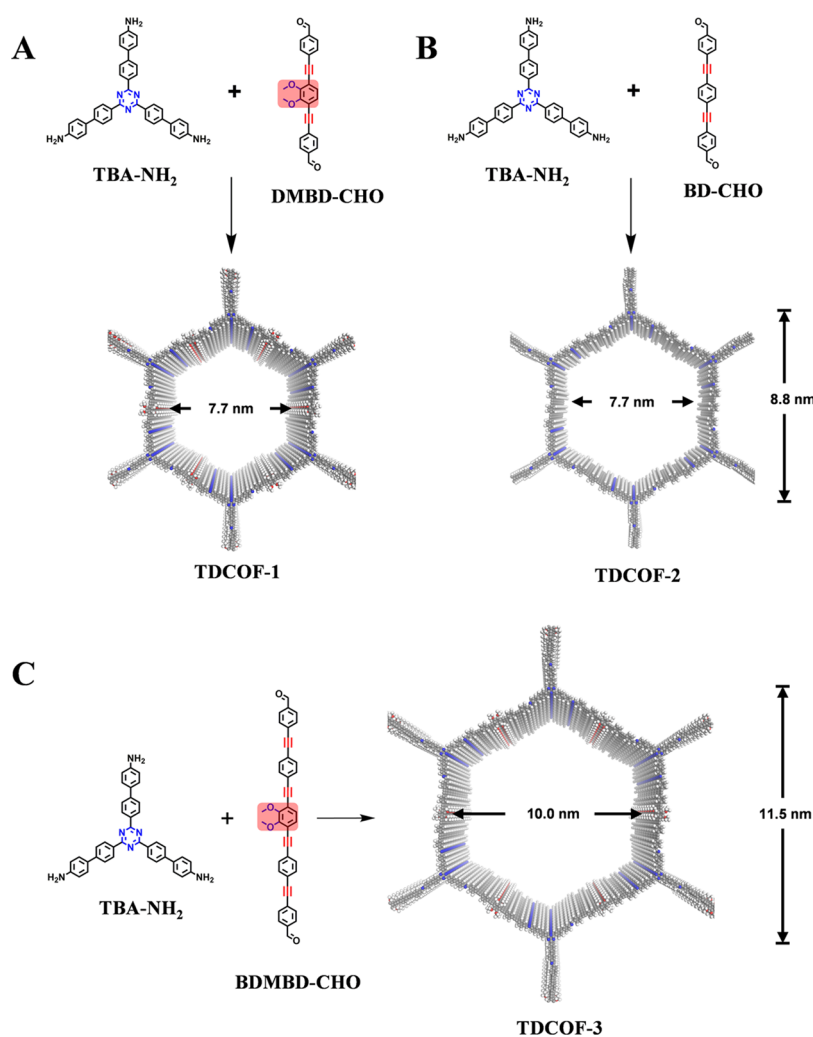


Figure 1. Synthesis routes of (A) TDCOF-1, (B) TDCOF-2, (C) TDCOF-3, and their corresponding perspective views of simulated eclipsed stacking models (C, gray; H, white; N, blue; O, red).

In addition, TDCOF-1 can be used as a shield to protect tyrosinase (TYR) ($5.5 \times 5.5 \times 5.6 \text{ nm}^3$) from heat-induced deactivation.

EXPERIMENTAL SECTION

In this work, all chemicals and solvents were commercially available and used without further treatments unless otherwise noted. 4',4'',4'''-(1,3,5-Triazine-2,4,6-triyl)tris([1,1'-biphenyl]-4-amine) (TBA-NH₂), 4,4'-(1,4-phenylenebis(ethyne-2,1-diyl))dibenzaldehyde (BD-CHO), and 5''-(4'-amino-[1,1'-biphenyl]-4-yl)-[1,1':4',1'':3'',1''':4''',1''''-quinquephenyl]-4,4''-diamine (TADPB-NH₂) were purchased from Jilin Chinese Academy of Science-Yanshen Technology Co., Ltd. Solvents including mesitylene, 1,4-dioxane, 1,2-dichlorobenzene, and *n*-butyl alcohol were purchased from Energy Chemical. The precursors of aldehyde monomers, including 1,4-diiodo-2,3-dimethoxybenzene, 1,4-diiodo-2,5-dimethoxybenzene, 4-ethynylbenzaldehyde, and ((4-iodophenyl)ethynyl)trimethylsilane were purchased from Tensus Biotech., Co., Ltd. The building blocks such as 4,4'-((2,3-dimethoxy-1,4-phenylene)bis(ethyne-2,1-diyl))dibenzaldehyde (DMBD-CHO), 4,4'-(((2,3-dimethoxy-1,4-phenylene)bis(ethyne-2,1-diyl))bis(4,1-phenylene))bis(ethyne-2,1-diyl)dibenzaldehyde (BDMBD-CHO), 4,4'-(((1,4-phenylenebis(ethyne-2,1-diyl))bis(4,1-phenylene))bis(ethyne-2,1-diyl))dibenzaldehyde (BBD-CHO), and 4,4'-(((2,5-dimethoxy-1,4-phenylene)bis(ethyne-2,1-diyl))bis(4,1-phenylene))bis(ethyne-2,1-diyl))dibenzaldehyde (BPMBD-CHO) were synthesized according to

the corresponding literature or with further modifications (see the [Supporting Information](#) for details).

Small-angle X-ray scattering (SAXS) was performed on the Xenocs Xeuss 3.0 system with a Cu K α X-ray source ($\lambda = 1.5418 \text{ \AA}$) at 25 °C. Structural modeling and Pawley refinement of TDCOFs were performed by using Materials Studio suite of programs to obtain the stacking models of TDCOFs and their corresponding lattice cell parameters. Nitrogen sorption isotherm measurements were carried out on a Kubo X1000 analyzer at 77 K in a P/P_0 pressure range from 10^{-5} to 1. Fourier transform infrared (FT-IR) spectra were collected in the range of 400–4000 cm^{-1} on a Bruker ALPHA spectrometer. Elemental analyses (EA) were performed on an Elementar UNICUBE elemental analyzer to obtain the contents of C, H, and N. Field-emission scanning electron microscopy (FE-SEM) images were obtained from a JEOL model JSM-7500F scanning electron microscope at 10 kV. High-resolution transmission electron microscopy (HRTEM) was performed on a JEOL JEM-2100Plus transmission electron microscope (LaB₆ filament). Thermogravimetric analysis (TGA) data were collected on a Netzsch STA449F5 analyzer at a heating rate of 10 K min^{-1} with a temperature range from 40 to 800 °C. ¹H NMR and ¹³C NMR spectra were obtained from a Bruker Advanced III 400 MHz NMR spectrometer in the correspondingly fitting deuterium-generation reagent. Solid-state ¹³C CP-MAS NMR spectra were collected on a JEOL ECZ600R/S3 NMR spectrometer.

Synthesis of TDCOF-1. A 10 mL glass ampoule was charged with TBA-NH₂ (17 mg, 0.03 mmol) and DMBD-CHO (18 mg, 0.045

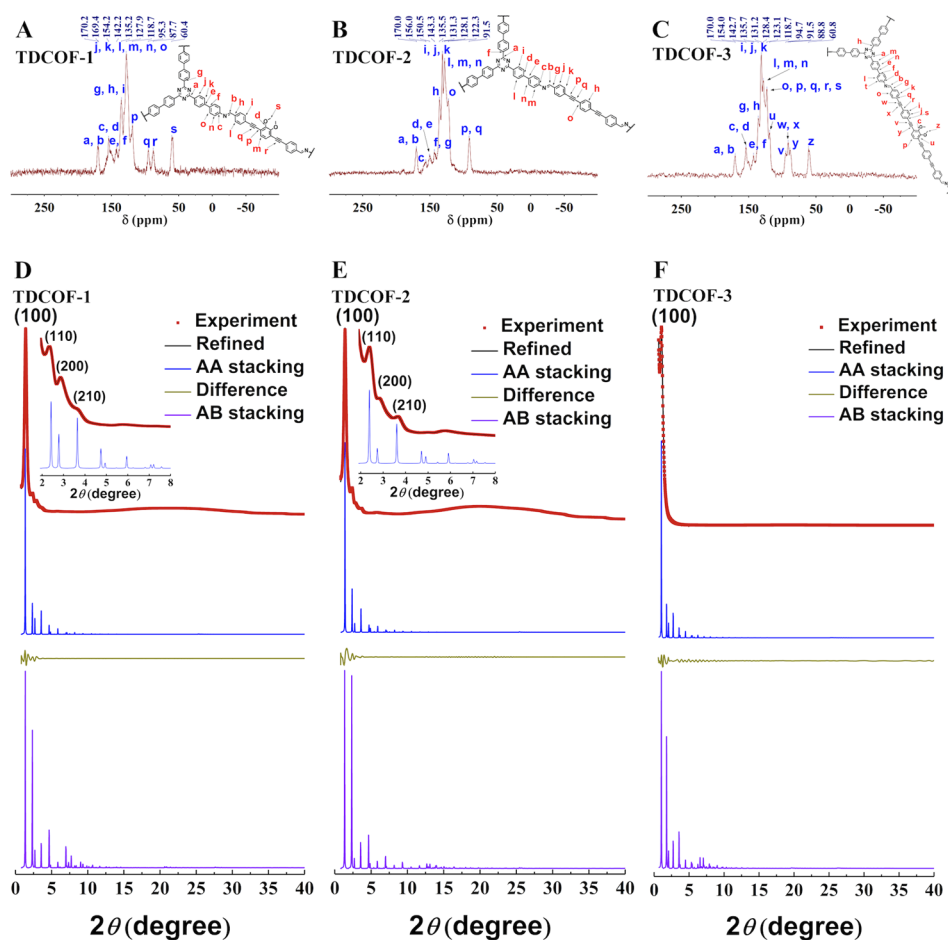


Figure 2. Solid-state ^{13}C CP/MAS NMR spectra of (A) TDCOF-1, (B) TDCOF-2, and (C) TDCOF-3. SAXS patterns of (D) TDCOF-1, (E) TDCOF-2, and (F) TDCOF-3, including experimental (red curves), Pawley refined (black curves) patterns and their difference (yellow curves), the simulated patterns for eclipsed AA stacking (blue curves), and AB stacking (purple curves). Insets: the corresponding partially enlarged patterns.

mmol); then, the mixtures of *o*-dichlorobenzene/*n*-BuOH (0.6/1.4 mL) were added. Then, the glass ampoule was sealed with parafilm and sonicated for 5 min. Subsequently, aqueous acetic acid (6 M, 400 μL) was added, and the glass ampoule was again sealed by parafilm and sonicated for 10 min, which was subsequently degassed through three freeze–pump–thaw cycles. After heating at 120 $^{\circ}\text{C}$ for 5 days, the precipitate was cooled to room temperature. The powder was collected and washed with tetrahydrofuran (THF) and methanol alternately by decantation and then exchanged with the corresponding solvents three times a day until the supernatant did not show obvious fluorescence under 365 nm UV light irradiation. Finally, the solid was further treated with supercritical CO_2 in a Tousimis Samdri PVT-3D critical point dryer (see the Supporting Information for details) and TDCOF-1 was obtained as a light-yellow powder (29 mg, 86% yield).

Synthesis of TDCOF-2. TDCOF-2 was prepared by a similar method, except that TBA-NH₂ (17 mg, 0.03 mmol) and BD-CHO (15 mg, 0.045 mmol) were used as monomers with a solvent of *o*-dichlorobenzene/*n*-BuOH (0.7/0.3 mL), and the amount of aqueous acetic acid was changed to 200 μL . TDCOF-2 was obtained as a yellow powder (25 mg, 82% yield).

Synthesis of TDCOF-3. TDCOF-3 was prepared through a similar method, except that TBA-NH₂ (12 mg, 0.02 mmol) and BDMBD-CHO (18 mg, 0.03 mmol) were used as monomers and mesitylene/1,4-dioxane (1.0/1.0 mL) was used as a solvent. TDCOF-3 was obtained as a yellow powder (19 mg, 67% yield).

To increase the crystallinity and surface area of the obtained TDCOFs, all of the synthesized samples were further treated with the corresponding reaction solvent under heating at 120 $^{\circ}\text{C}$ for another 5 days to allow error-checking and self-repairing. The resultant powders

were washed and activated via organic solvent exchange and supercritical CO_2 treatment.

RESULTS AND DISCUSSION

TDCOF-1, TDCOF-2, and TDCOF-3 were synthesized via co-condensation of amido block (TBA-NH₂) with DMBD-CHO, BD-CHO, and BDMBD-CHO, respectively, under solvothermal conditions (Figure 1). All these TDCOFs are imine-linked hexagonal mesoporous COFs.

The chemical structures of the TDCOFs were characterized. Solid-state ^{13}C cross-polarization magic angle spinning nuclear magnetic resonance (CP/MAS NMR) spectra reveal that these TDCOFs present all of the characteristic signals of the carbons that can be assigned to their corresponding chemical structures (Figure 2A–C). The signal peaks at 1626 cm^{-1} observed in the Fourier transform infrared (FT-IR) spectra of TDCOFs are assigned to the stretching vibration of C=N in triazine rings and imine linkages (Figure S1). The disappearance of the peaks assigned to the amino groups and the significantly weakened C=O stretching band (1700 cm^{-1}) reveals high polymerization degrees for TDCOFs (Figure S1). Elemental analysis data show that the C, H, and N contents are in agreement with the theoretical values (Table S1). Thermogravimetric analysis curves demonstrate that these TDCOFs are thermally stable up to ~ 500 $^{\circ}\text{C}$ (Figure S2). The particle morphologies of TDCOFs are shown in Figure S3.

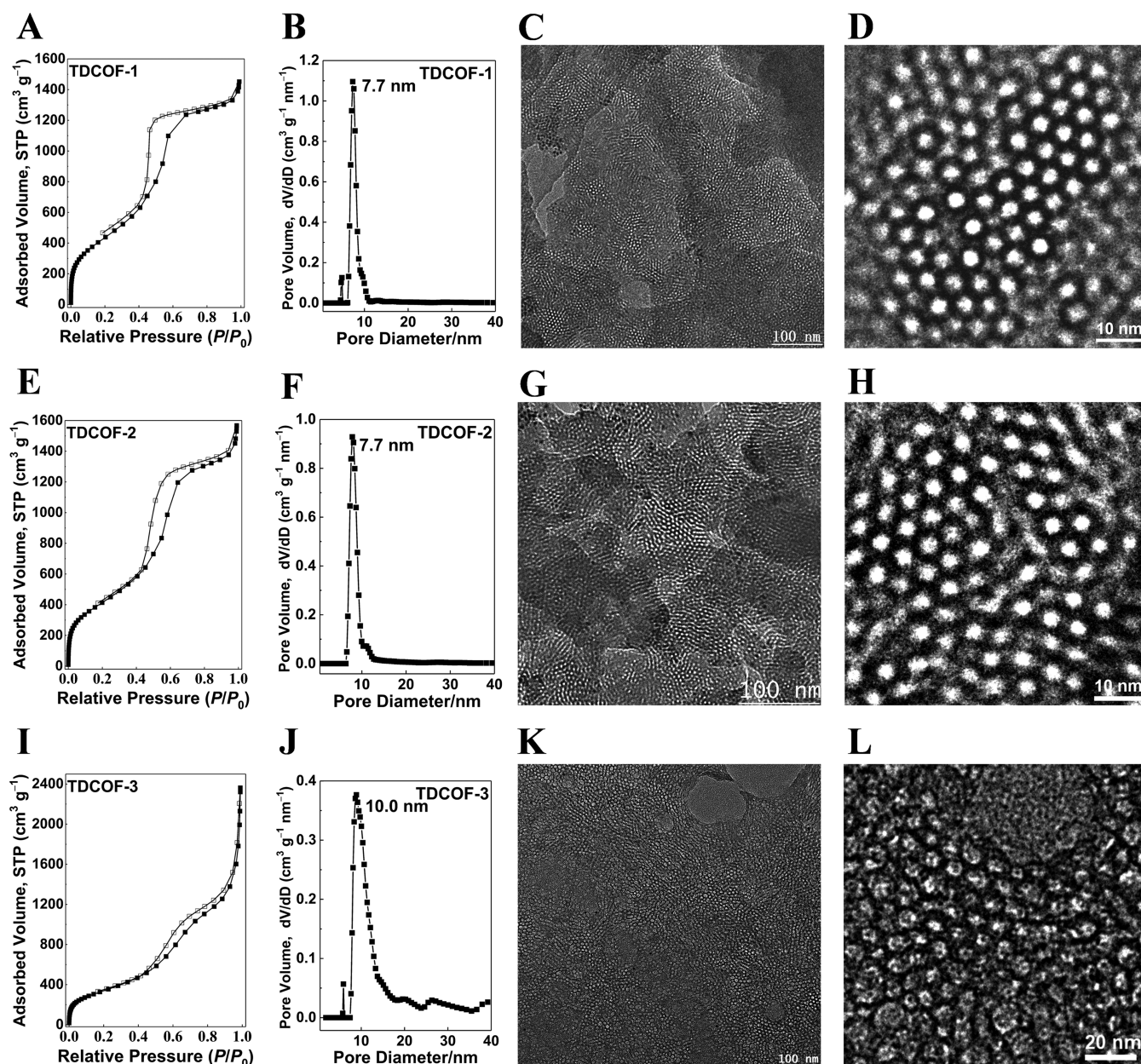


Figure 3. Nitrogen sorption isotherms, pore size distribution curves, and HRTEM images of (A–D) TDCOF-1, (E–H) TDCOF-2, and (I–L) TDCOF-3.

The crystallinities of these TDCOFs were characterized by small-angle X-ray scattering (SAXS) measurements. Pawley refinements were performed to deduce the lattice parameters from the corresponding SAXS patterns (Figure 2D–F, Tables S4, S6, and S7). 2D polymeric sheets with extended hexagonal polygons were constructed by placing the amido and aldehydic blocks at the vertices and edges, respectively. Then, AA stacking and AB stacking crystal models were further built by placing the 2D sheets in an eclipsed or staggered fashion within the obtained cells, respectively, followed by geometry optimization. It should be noted that for TDCOF-1 and TDCOF-3 in AA stacking modes, whether the methoxy groups are alternately arranged at the two sides of the walls (the crystal models are denoted as TDCOF-1-A and TDCOF-3-A) or anchored at the same side of the benzene ring (the crystal models are denoted as TDCOF-1-S and TDCOF-3-S) along

the 1D pore channels, the XRD simulation results are not influenced.

For TDCOF-1 and -2, the enlarged SAXS patterns are in good agreement with the simulated patterns of eclipsed structure, which can reproduce both the position and intensity of the experimental peaks (Figure 2D,E). The sharp SAXS peak of TDCOF-1 at $2\theta = 1.47^\circ$ can be assigned to the (100) facet of a highly regular lattice that is stacked in a hexagonal orientation. The other minor peaks at $2\theta = 2.46, 2.82,$ and 3.70° are assigned to the (110), (200), and (210) facets, respectively (Figure 2D, red curve, Figure S4). Similarly, the SAXS peaks of TDCOF-2 appear at $2\theta = 1.46, 2.45, 2.81,$ and 3.70° are attributed to the (100), (110), (200), and (210) facets, respectively (Figure 2E, red curve, Figure S5), while an intense SAXS peak at $2\theta = 1.05^\circ$ assigned to the (100) facet is observed for TDCOF-3 (Figure 2F, red curve, Figure S6). In contrast, for the AB stacking models, the relative intensity of

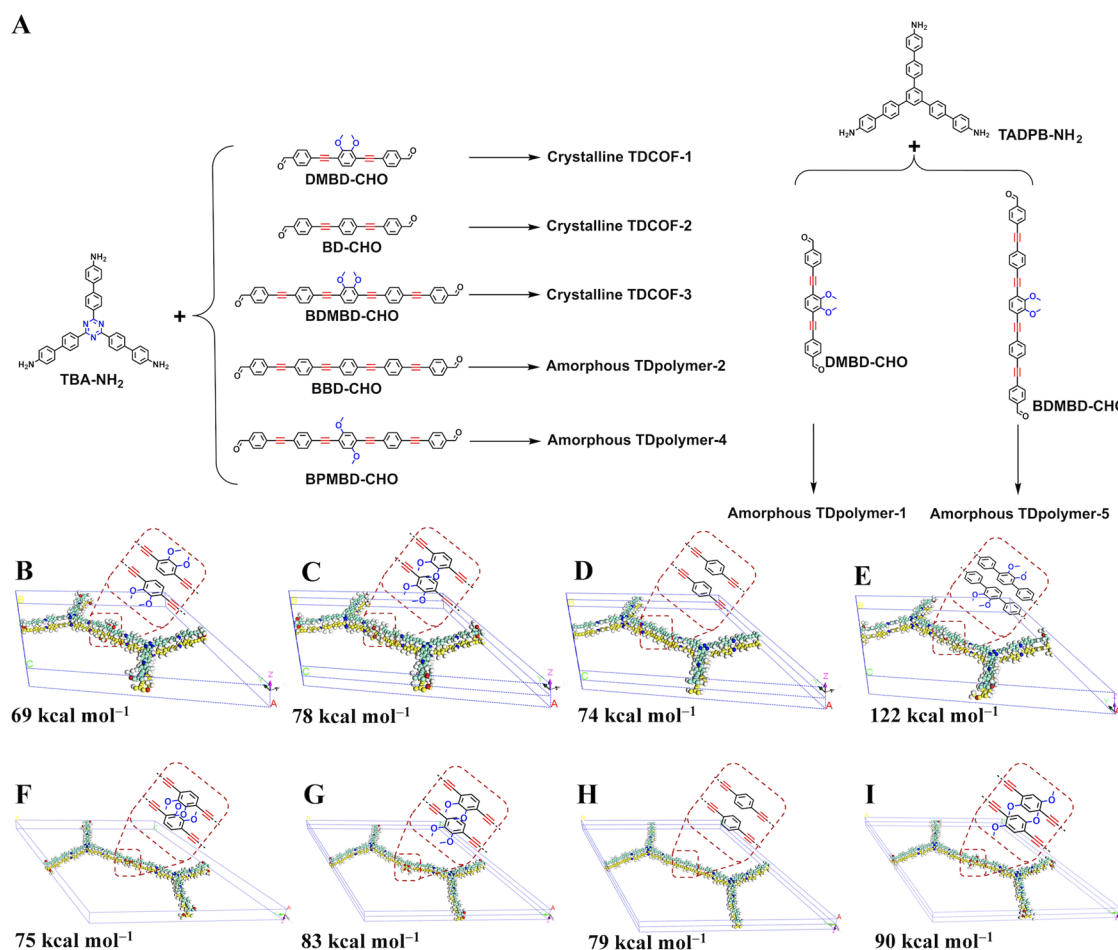


Figure 4. (A) Schematic representation of the syntheses of TDCOFs and TDpolymers. Crystal cell models of (B) TDCOF-1-A, (C) TDCOF-1-S, (D) TDCOF-2, (E) TDpolymer-3-A, (F) TDCOF-3-A, (G) TDCOF-3-S, (H) TDpolymer-2, (I) TDpolymer-4, and their corresponding nonbond energy per monolayer in the unit cell.

peaks assigned to (100) and (110) should be similar due to the crystal symmetry, which disagrees with the experimental results (Figure 2D,E, purple curves). Compared to those for TDCOF-1 and -2, the absence of relatively high-angle scattering peaks for TDCOF-3 suggests its relatively low periodicity owing to the difficulty in crystallization in obtaining such a large mesoporous COF.

In addition, we constructed the stacking models of TDCOF-1 with varied interlayer slipped distances (0.4, 0.8, 4, 8, and 32 Å) along different directions (Figure S7). The simulated XRD patterns do not show significant differences except for the model with a 32 Å offset, yet the calculated nonbond energy results indicate the models with eclipsed stacking or very slightly offset (0.4 Å) are thermodynamically favorable. The pore structure features of TDCOFs were further confirmed by N_2 sorption analyses and HRTEM.

Nitrogen sorption isotherm measurements were performed at 77 K to investigate the porosity of TDCOFs, and the samples were activated before measurements (see the Supporting Information for details). All of the TDCOFs exhibit typical type IV isotherms with high starting-point values of the relative pressure at the second step (Figure 3A,E,I), suggesting that they possess relatively large mesopores.^{52,59} Simultaneously, pore size distributions (Figure 3B,F,J) were calculated based on quenched solid density functional theory (QSDFT). Herein, pore widths of 7.7, 7.7,

and 10.0 nm dominate the pore size distribution profiles of TDCOF-1, TDCOF-2, and TDCOF-3, respectively, which is in agreement with the predicted pore sizes deduced from the eclipsed stacking models. Therefore, the pore size distributions further support the formation of eclipsed stacking structures rather than staggered crystalline or interpenetrated amorphous forms. The Brunauer–Emmett–Teller (BET) specific surface areas are determined to be 1665, 1560, and 1270 $m^2 g^{-1}$ for TDCOF-1, -2, and -3, respectively (Figure S8). The experimentally obtained values of surface areas are lower than the theoretical values (details are described in SI), which may indicate that there remain defects and/or blocked pores in the obtained COFs. Furthermore, the pore volumes are calculated based on the N_2 sorption uptake at $P/P_0 = 0.9$ by assuming all of the pores in the adsorbents are filled with condensed gas; the calculated pore volumes are directly influenced by the pore sizes. As a result, the pore volumes of TDCOF-1, -2, and -3 are calculated to be 2.02, 2.08, and 2.13 $cm^3 g^{-1}$, respectively, all of which are much higher than the reported COFs with smaller pores and even with higher surface areas (Table S3). Similar results were found in the IRMOF-74 series, whose pore volumes mainly increase with the extending of the pore widths irrespective of the BET surface area changes.

Moreover, the well-aligned hexagonal mesopores can be directly visualized by HRTEM, especially for TDCOF-1 and

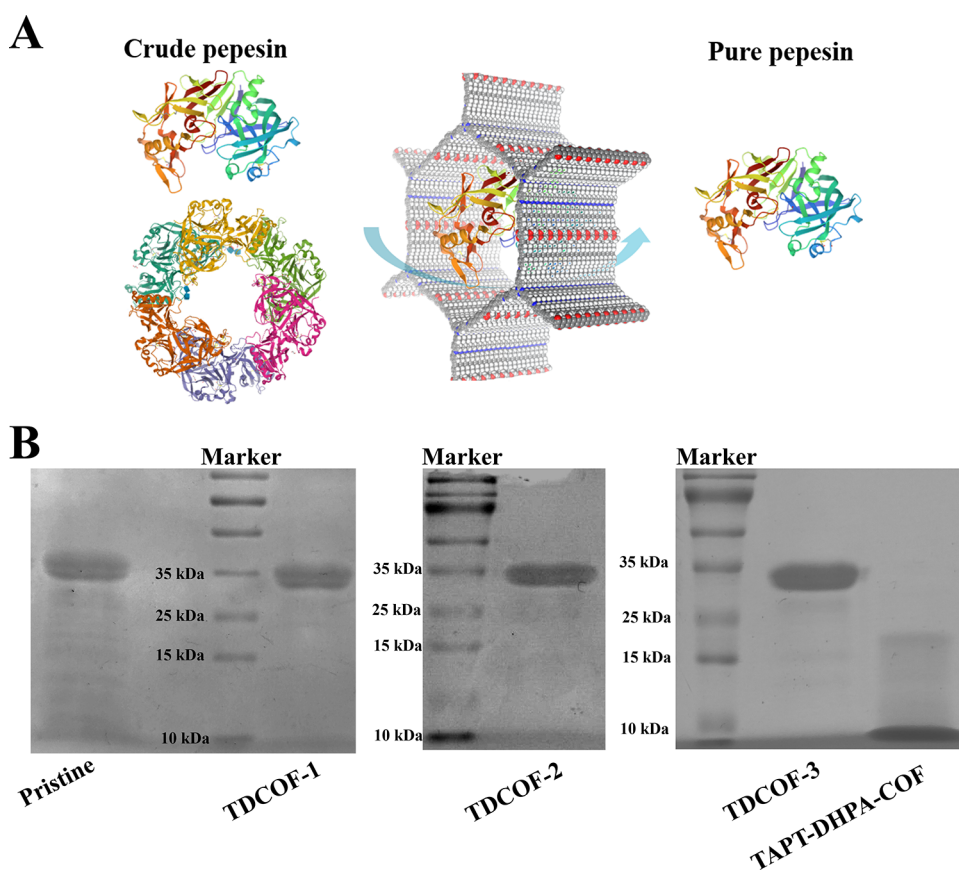


Figure 5. (A) Schematic representation of the separation of pepsin by TDCOFs. (B) SDS-PAGE results of the crude pepsin and the eluents after column separation by TDCOFs and TAPT-DHPA-COF.

TDCOF-2 (Figures 3C,D,G,H,K,L and S9). Although lots of grain boundaries between the crystalline domains are found, they do not influence the large mesoporous structural nature of the TDCOFs. For TDCOF-3, less uniform pores are observed owing to its lower crystallinity as well as lower tolerance toward high-energy electrons.^{60,61}

The chemical stabilities of these TDCOFs were examined by immersing the samples in organic solvents (including tetrahydrofuran, methanol, dimethylformamide) and aqueous HCl solution (pH = 1) at 40 °C for 24 h. The FT-IR spectra, SAXS profiles, and nitrogen sorption isotherms show no obvious changes after the treatment (Figures S10–S12), revealing their chemical robustness. In comparison, the MOF-74 families with large pores show relatively weak hydrostability.⁶²

To further clarify the role of triazine, alkynyl, and the asymmetric ortho-dimethoxy of the building blocks on the construction of periodical large-mesopore frameworks, we performed controlled experiments and theoretical energy calculations.

First, we utilized TADPB-NH₂, where the triazine species in TBA-NH₂ was substituted by benzene ring, to react with DMBD-CHO and BDMBD-CHO (Figure 4A, Scheme S5). The products, TDpolymer-1 and -5, obtained under different solvothermal conditions all exhibit low BET surface area with wide pore size distribution. In addition, although BD-CHO was successfully applied to prepare the COF with a 7.7 nm pore width, we could not further obtain the COFs with a 10.0 nm pore width via the extension of the monomer length, i.e., using BBD-CHO (without methoxy groups) and BDMBD-

CHO (with para-dimethoxy groups) to react with TBA-NH₂ (Figure 4A, Scheme S5, the product is denoted as TDpolymer-2 and TDpolymer-4, respectively).

Then, we built the corresponding crystal structures of TDCOFs (denoted as TDCOF-1-A, TDCOF-1-S, TDCOF-2, TDCOF-3-A, and TDCOF-3-S) and TDpolymers in AA stacking modes (denoted as TDpolymer-1-A, TDpolymer-2, TDpolymer-3-A, TDpolymer-4, and TDpolymer-5-A) based on the reticular chemistry (Figures 4B–I and S13). Table S2 shows the nonbond energy per monolayer in the unit cell of different structures or stacking modes, which are calculated by a force field method based on the universal force field. Since the dynamic covalent chemistry applied in the COF preparation favored the products with higher thermodynamic stability, lowering nonbond energy was beneficial for the formation of the crystalline products. Among the crystal cell models with similar pore sizes that we screened, COFs with alternately arranged methoxy groups showed the lowest nonbond energy. It was attributed to the fact that the dimethoxy groups anchoring at the same side of the benzene ring led to local polarization-induced interlayer interaction enhancement. In addition, compared with the benzene ring, the triazine ring possesses smaller steric hindrance between adjacent layers, leading to a much higher nonbond energy of TDpolymer-1-A compared with TDCOF-1-A. Similarly, the alkynyl species with sp hybrid C atoms are beneficial to increase the planarity and reduce the steric hindrance of the building units. To verify this assumption, we used phenyl groups to substitute the alkynyl group in DMBD-CHO to build a COF model (termed as TDpolymer-3-A, Scheme S7) with alternative AA stacking.

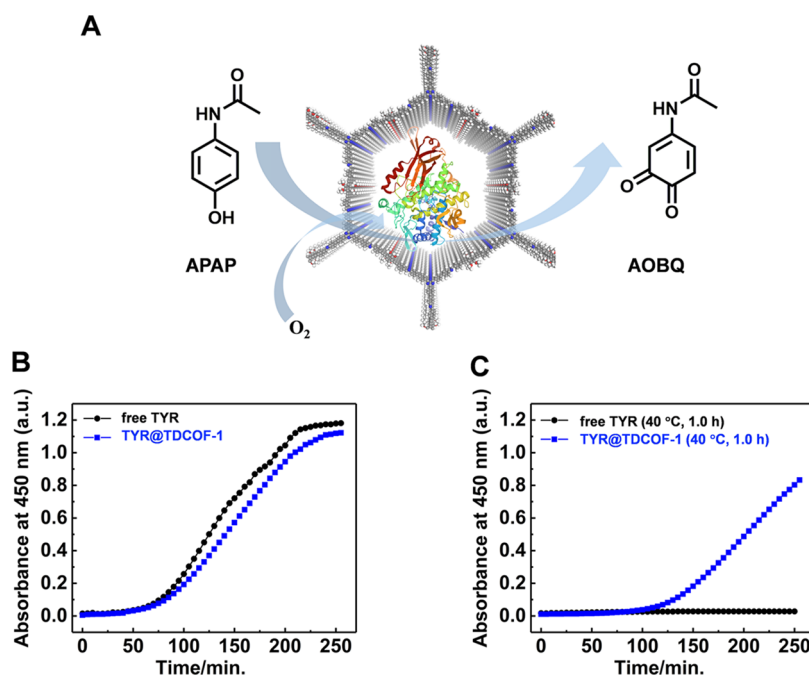


Figure 6. (A) Schematic representation of the loaded TYR in TDCOF-1 for catalyzing the oxidation of APAP. (B) Generation of AOBQ catalyzed by free TYR (black curve) and TYR@TDCOF-1 (blue curve) at room temperature. (C) Catalytic performance of free TYR (black curve) and TYR@TDCOF-1 (blue curve) after treatment at 40 °C for an hour.

The resultant optimized model adopts twisted nonplanar sheets with large nonbond energy. These thermodynamic energy comparisons as well as the successful preparation of TDCOF-1, TDCOF-2, and TDCOF-3 and the failures to experimentally obtain crystalline TDpolymer-1, -2, -4, and -5 prove the importance of controlling the conformational rigidity, reducing the steric hindrance, and introducing appropriate polarity of the building blocks for constructing COFs with large pore apertures.

As a proof of concept, we verified the accessibility of pore apertures of these TDCOFs to large biomolecules. We first performed the inclusion experiments of myoglobin ($2.1 \times 3.5 \times 4.4 \text{ nm}^3$) using TDCOF-1, -2, and -3. The adsorption capacities of these TDCOFs were monitored by measuring the absorbance of the supernatant with ultraviolet–visible (UV–vis) spectrophotometry (Figure S15). A continuous decrease of the myoglobin in their supernatants was found, indicating the successful inclusion of myoglobin into the pore apertures of TDCOFs. The myoglobin uptake capacities are calculated to be 1.50, 0.56, and 0.72 mg per milligram of TDCOF-1, -2, and -3, respectively.

Taking advantage of the accessible large mesopores of TDCOFs, we applied them as column-packing materials in the separation of the commercially purchased crude pepsin in PBS solution (pH = 5). While the dimension of the pepsin published in the protein data bank (PDB) was $3.6 \times 5.5 \times 7.4 \text{ nm}^3$,⁶³ the pepsin favored the forming hydration shell presenting a larger dimension. The crude pepsin showed wide molecular weight distributions as determined by sodium dodecyl sulfate–polyacrylamide gel electrophoresis (SDS–PAGE). After separation by TDCOFs, almost pure pepsin with a molecular weight of 35 kDa could be obtained (Figure 5). As a control experiment, only low-molecular-weight components could be found in the eluents using TAPT-DHPA-COF with 3.1 nm pore apertures (Figure S14) for pepsin separation (Figure 5). It is hypothesized that pepsin

molecules were trapped in the surface pores of TAPT-DHPA-COF.

To further demonstrate the importance of the large pore aperture, we utilized TDCOF-1 as a carrier to load tyrosinase (TYR) ($5.5 \times 5.5 \times 5.6 \text{ nm}^3$) for catalyzing the oxidation reaction of paracetamol (Figure 6A), the product of which was an active ingredient of Tylenol.⁶⁴ The catalytic kinetic curves of free TYR and TYR@TDCOF-1 were assessed by monitoring the absorbance intensity at 450 nm, which belonged to the absorption of 4-acetamido-*o*-benzoquinone (AOBQ) product. As shown in Figure 6B, TYR@TDCOF-1 shows an almost equal catalytic activity compared with free TYR. We further proved the protection effect of COF on the enzyme's thermal stability. The free TYR and TYR@TDCOF-1 were treated at 40 °C for 1 h before the catalytic reaction. TYR@TDCOF-1 still showed high activity toward paracetamol oxidation despite a slight hysteric production of AOBQ. In sharp contrast, free TYR completely lost its catalytic activity due to heat-induced deactivation (Figure 6C). The above results demonstrate that the large mesoporous COFs can efficiently load large enzymes and serve as shields to avoid enzyme deactivation under rigorous conditions.⁶⁵

CONCLUSIONS

We have extended the record pore width of COFs from 5.8 to 10.0 nm. These large-mesopore TDCOFs exhibit high crystallinity, permanent porosity, and high thermal and chemical stabilities. The large pore apertures and robustness impart these TDCOFs with abilities to encapsulate myoglobin, separate pepsin under acidic conditions, and load TYR for catalyzing the oxidation reaction of paracetamol. These studies shed light on the raising of the upper limit of pore size of COFs, providing a promising future for biological applications.

■ ASSOCIATED CONTENT

SI Supporting Information

The Supporting Information is available free of charge at <https://pubs.acs.org/doi/10.1021/jacs.2c00584>.

Materials and methods, characterization data, and FT-IR spectra of (A) TDCOF-1, (B) TDCOF-2, (C) TDCOF-3, and their corresponding monomers; SEM images of (A, D) TDCOF-1, (B, E) TDCOF-2, and (C, F) TDCOF-3 at different magnification ratios; BET plots of (A) TDCOF-1, (B) TDCOF-2, and (C) TDCOF-3 from nitrogen adsorption data; TEM images of TDCOF-1 (A–D), TDCOF-2 (E–H), and TDCOF-3 (I–L); crystal cell models of (A) TDpolymer-1-A and (B) TDpolymer-5-A and their corresponding nonbond energy per monolayer in the unit cell; elemental analysis data of TDCOF-1, TDCOF-2, and TDCOF-3; summary of the BET surface areas, pore volumes, and pore diameters of TDCOFs, IRMOFs, and some representative COFs; atomistic coordinates of the refined unit cell parameters for TDCOF-1-A; and atomistic coordinates of the unit cell parameters for TDpolymer-5-A (Figures S1–S15 and Tables S1–S13) (PDF)

■ AUTHOR INFORMATION

Corresponding Author

Xiao Feng – Beijing Key Laboratory of Photoelectronic/Electrophotonic Conversion Materials, Key Laboratory of Cluster Science, Ministry of Education, Advanced Technology Research Institute (Jinan), Frontiers Science Center for High Energy Material, School of Chemistry and Chemical Engineering, Beijing Institute of Technology, Beijing 100081, P. R. China; orcid.org/0000-0002-3212-3051; Email: fengxiao86@bit.edu.cn

Authors

Zhenjie Mu – Beijing Key Laboratory of Photoelectronic/Electrophotonic Conversion Materials, Key Laboratory of Cluster Science, Ministry of Education, Advanced Technology Research Institute (Jinan), Frontiers Science Center for High Energy Material, School of Chemistry and Chemical Engineering, Beijing Institute of Technology, Beijing 100081, P. R. China

Yuhao Zhu – Beijing Key Laboratory of Photoelectronic/Electrophotonic Conversion Materials, Key Laboratory of Cluster Science, Ministry of Education, Advanced Technology Research Institute (Jinan), Frontiers Science Center for High Energy Material, School of Chemistry and Chemical Engineering, Beijing Institute of Technology, Beijing 100081, P. R. China

Bixiao Li – Beijing Key Laboratory of Photoelectronic/Electrophotonic Conversion Materials, Key Laboratory of Cluster Science, Ministry of Education, Advanced Technology Research Institute (Jinan), Frontiers Science Center for High Energy Material, School of Chemistry and Chemical Engineering, Beijing Institute of Technology, Beijing 100081, P. R. China

Anwang Dong – Beijing Key Laboratory of Photoelectronic/Electrophotonic Conversion Materials, Key Laboratory of Cluster Science, Ministry of Education, Advanced Technology Research Institute (Jinan), Frontiers Science Center for High Energy Material, School of Chemistry and Chemical

Engineering, Beijing Institute of Technology, Beijing 100081, P. R. China; orcid.org/0000-0001-9068-6015

Bo Wang – Beijing Key Laboratory of Photoelectronic/Electrophotonic Conversion Materials, Key Laboratory of Cluster Science, Ministry of Education, Advanced Technology Research Institute (Jinan), Frontiers Science Center for High Energy Material, School of Chemistry and Chemical Engineering, Beijing Institute of Technology, Beijing 100081, P. R. China; orcid.org/0000-0001-9092-3252

Complete contact information is available at:

<https://pubs.acs.org/10.1021/jacs.2c00584>

Author Contributions

The manuscript was written through contributions of all authors. All authors have given approval to the final version of the manuscript.

Notes

The authors declare no competing financial interest.

■ ACKNOWLEDGMENTS

This work was financially supported by the National Natural Science Foundation of China (Grant Nos. 22171022, 21922502, 21625102, and 21971017), the National Key Research and Development Program of China (2020YFB1506300), the Beijing Institute of Technology Research Fund Program, and Testing Center of Beijing Institute of Technology. The authors thank Dr. Zhiye Zhong and Prof. Yanhang Ma (ShanghaiTech University) for their help with TEM measurements.

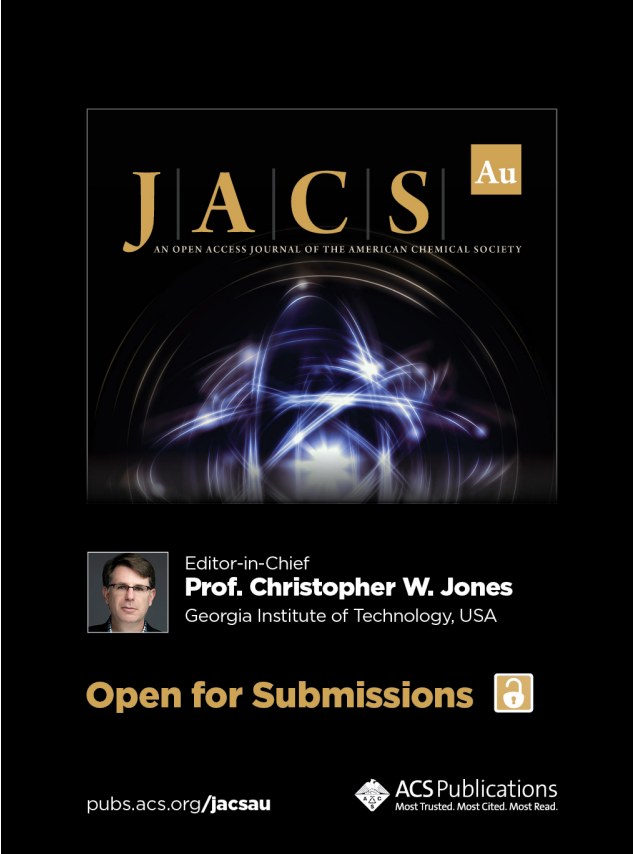
■ ABBREVIATIONS

COFs	covalent organic frameworks
TBA-NH ₂	4',4'',4'''-(1,3,5-triazine-2,4,6-triyl)tris([1,1'-biphenyl]-4-amine))
DMBD-CHO	4,4'-((2,3-dimethoxy-1,4-phenylene)bis(ethyne-2,1-diyl))-dibenzaldehyde
BD-CHO	4,4'-(1,4-phenylenebis(ethyne-2,1-diyl))dibenzaldehyde
BDMBD-CHO	4,4'-(((2,3-dimethoxy-1,4-phenylene)bis(ethyne-2,1-diyl))-bis(4,1-phenylene))bis(ethyne-2,1-diyl)dibenzaldehyde
TADPB-NH ₂ , BBD-CHO	5''-(4'-amino-[1,1'-biphenyl]-4-yl)-[1,1':4',1'':3'',1''':4''',1''''-quinquephenyl]-4,4''-diamine, 4,4'-(((1,4-phenylenebis(ethyne-2,1-diyl))bis(4,1-phenylene))bis(ethyne-2,1-diyl))dibenzaldehyde
SAXS	small-angle X-ray scattering
QSDFT	quenched solid density functional theory
SSA	specific surface area
BET	Brunauer–Emmett–Teller
HRTEM	high-resolution transmission electron microscopy
FTIR	Fourier transform infrared spectroscopy
PDB	protein data bank
TYR	tyrosinase
AOBQ	4-acetamido- <i>o</i> -benzoquinone


REFERENCES

- (1) Long, J. R.; Yaghi, O. M. The Pervasive Chemistry of Metal–Organic Frameworks. *Chem. Soc. Rev.* **2009**, *38*, 1213–1214.
- (2) O’Keeffe, M. Design of MOFs and Intellectual Content in Reticular Chemistry: A Personal View. *Chem. Soc. Rev.* **2009**, *38*, 1215–1217.
- (3) Geng, K.; He, T.; Liu, R.; Dalapati, S.; Tan, K. T.; Li, Z.; Tao, S.; Gong, Y.; Jiang, Q.; Jiang, D. Covalent Organic Frameworks: Design, Synthesis, and Functions. *Chem. Rev.* **2020**, *120*, 8814–8933.
- (4) Sun, Q.; Dai, Z.; Meng, X.; Xiao, F.-S. Porous Polymer Catalysts with Hierarchical Structures. *Chem. Soc. Rev.* **2015**, *44*, 6018–6034.
- (5) Ben, T.; Qiu, S. Porous Aromatic Frameworks: Synthesis, Structure and Functions. *CrystEngComm* **2013**, *15*, 17–26.
- (6) Côté, A. P.; Benin, A. I.; Ockwig, N. W.; Keffe, M.; Matzger, A. J.; Yaghi, O. M. Porous, Crystalline, Covalent Organic Frameworks. *Science* **2005**, *310*, 1166–1170.
- (7) Feng, X.; Ding, X.; Jiang, D. Covalent Organic Frameworks. *Chem. Soc. Rev.* **2012**, *41*, 6010–6022.
- (8) Ding, S. Y.; Wang, W. Covalent Organic Frameworks (COFs): From Design to Applications. *Chem. Soc. Rev.* **2013**, *42*, 548–568.
- (9) Huang, N.; Wang, P.; Jiang, D. Covalent Organic Frameworks: A Materials Platform for Structural and Functional Designs. *Nat. Rev. Mater.* **2016**, *1*, No. 16068.
- (10) Segura, J. L.; Mancheno, M. J.; Zamora, F. Covalent Organic Frameworks Based on Schiff-Base Chemistry: Synthesis, Properties and Potential Applications. *Chem. Soc. Rev.* **2016**, *45*, 5635–5671.
- (11) Diercks, C. S.; Yaghi, O. M. The Atom, the Molecule, and the Covalent Organic Framework. *Science* **2017**, *355*, No. eaal1585.
- (12) Lohse, M. S.; Bein, T. Covalent Organic Frameworks: Structures, Synthesis, and Applications. *Adv. Funct. Mater.* **2018**, *28*, No. 1705553.
- (13) Kandambeth, S.; Dey, K.; Banerjee, R. Covalent Organic Frameworks: Chemistry Beyond the Structure. *J. Am. Chem. Soc.* **2019**, *141*, 1807–1822.
- (14) Huang, X.; Sun, C.; Feng, X. Crystallinity and Stability of Covalent Organic Frameworks. *Sci. China: Chem.* **2020**, *63*, 1367–1390.
- (15) Han, S. S.; Furukawa, H.; Yaghi, O. M.; Goddard, W. A. Covalent Organic Frameworks as Exceptional Hydrogen Storage Materials. *J. Am. Chem. Soc.* **2008**, *130*, 11580–11581.
- (16) Kuhn, P.; Antonietti, M.; Thomas, A. Porous, Covalent Triazine-Based Frameworks Prepared by Ionothermal Synthesis. *Angew. Chem., Int. Ed.* **2008**, *47*, 3450–3453.
- (17) Furukawa, H.; Yaghi, O. M. Storage of Hydrogen, Methane, and Carbon Dioxide in Highly Porous Covalent Organic Frameworks for Clean Energy Applications. *J. Am. Chem. Soc.* **2009**, *131*, 8875–8883.
- (18) Yu, J.-T.; Chen, Z.; Sun, J.; Huang, Z.-T.; Zheng, Q.-Y. Cyclotricatechylene Based Porous Crystalline Material: Synthesis and Applications in Gas Storage. *J. Mater. Chem.* **2012**, *22*, 5369–5373.
- (19) Gottschling, K.; Stegbauer, L.; Savasci, G.; Prisco, N. A.; Berkson, Z. J.; Ochsenfeld, C.; Chmelka, B. F.; Lotsch, B. V. Molecular Insights into Carbon Dioxide Sorption in Hydrazone-Based Covalent Organic Frameworks with Tertiary Amine Moieties. *Chem. Mater.* **2019**, *31*, 1946–1955.
- (20) Ding, S.-Y.; Gao, J.; Wang, Q.; Zhang, Y.; Song, W.-G.; Su, C.-Y.; Wang, W. Construction of Covalent Organic Framework for Catalysis: Pd/COF-Lzu1 in Suzuki–Miyaura Coupling Reaction. *J. Am. Chem. Soc.* **2011**, *133*, 19816–19822.
- (21) Xu, H.; Chen, X.; Gao, J.; Lin, J.; Addicoat, M.; Irlle, S.; Jiang, D. Catalytic Covalent Organic Frameworks Via Pore Surface Engineering. *Chem. Commun.* **2014**, *50*, 1292–1294.
- (22) Vyas, V. S.; Haase, F.; Stegbauer, L.; Savasci, G.; Podjaski, F.; Ochsenfeld, C.; Lotsch, B. V. A Tunable Azine Covalent Organic Framework Platform for Visible Light-Induced Hydrogen Generation. *Nat. Commun.* **2015**, *6*, No. 8508.
- (23) Xu, H.; Gao, J.; Jiang, D. Stable, Crystalline, Porous, Covalent Organic Frameworks as a Platform for Chiral Organocatalysts. *Nat. Chem.* **2015**, *7*, 905–912.
- (24) Sun, Q.; Aguila, B.; Perman, J.; Nguyen, N.; Ma, S. Flexibility Matters: Cooperative Active Sites in Covalent Organic Framework and Threaded Ionic Polymer. *J. Am. Chem. Soc.* **2016**, *138*, 15790–15796.
- (25) Wang, X.; Han, X.; Zhang, J.; Wu, X.; Liu, Y.; Cui, Y. Homochiral 2d Porous Covalent Organic Frameworks for Heterogeneous Asymmetric Catalysis. *J. Am. Chem. Soc.* **2016**, *138*, 12332–12335.
- (26) Mu, M.; Wang, Y.; Qin, Y.; Yan, X.; Li, Y.; Chen, L. Two-Dimensional Imine-Linked Covalent Organic Frameworks as a Platform for Selective Oxidation of Olefins. *ACS Appl. Mater. Interfaces* **2017**, *9*, 22856–22863.
- (27) Yan, S.; Guan, X.; Li, H.; Li, D.; Xue, M.; Yan, Y.; Valtchev, V.; Qiu, S.; Fang, Q. Three-Dimensional Salphen-Based Covalent–Organic Frameworks as Catalytic Antioxidants. *J. Am. Chem. Soc.* **2019**, *141*, 2920–2924.
- (28) Liu, G.; Sheng, J.; Zhao, Y. Chiral Covalent Organic Frameworks for Asymmetric Catalysis and Chiral Separation. *Sci. China: Chem.* **2017**, *60*, 1015–1022.
- (29) Wan, S.; Guo, J.; Kim, J.; Ihee, H.; Jiang, D. A Belt-Shaped, Blue Luminescent, and Semiconducting Covalent Organic Framework. *Angew. Chem., Int. Ed.* **2008**, *47*, 8826–8830.
- (30) Bertrand, G. H.; Michaelis, V. K.; Ong, T. C.; Griffin, R. G.; Dinca, M. Thiophene-Based Covalent Organic Frameworks. *Proc. Natl. Acad. Sci. U.S.A.* **2013**, *110*, 4923–4928.
- (31) Dogru, M.; Handloser, M.; Auras, F.; Kunz, T.; Medina, D.; Hartschuh, A.; Knochel, P.; Bein, T. A Photoconductive Thienothio-phenene-Based Covalent Organic Framework Showing Charge Transfer Towards Included Fullerene. *Angew. Chem., Int. Ed.* **2013**, *52*, 2920–2924.
- (32) Aiyappa, H. B.; Thote, J.; Shinde, D. B.; Banerjee, R.; Kurungot, S. Cobalt-Modified Covalent Organic Framework as a Robust Water Oxidation Electrocatalyst. *Chem. Mater.* **2016**, *28*, 4375–4379.
- (33) Guo, H.; Wang, J.; Fang, Q.; Zhao, Y.; Gu, S.; Zheng, J.; Yan, Y. A Quaternary-Ammonium-Functionalized Covalent Organic Framework for Anion Conduction. *CrystEngComm* **2017**, *19*, 4905–4910.
- (34) Lin, C.-Y.; Zhang, L.; Zhao, Z.; Xia, Z. Design Principles for Covalent Organic Frameworks as Efficient Electrocatalysts in Clean Energy Conversion and Green Oxidizer Production. *Adv. Mater.* **2017**, *29*, No. 1606635.
- (35) Montoro, C.; Rodríguez-San-Miguel, D.; Polo, E.; Escudero-Cid, R.; Ruiz-González, M. L.; Navarro, J. A. R.; Ocón, P.; Zamora, F. Ionic Conductivity and Potential Application for Fuel Cell of a Modified Imine-Based Covalent Organic Framework. *J. Am. Chem. Soc.* **2017**, *139*, 10079–10086.
- (36) Cao, L.; Wu, H.; Cao, Y.; Fan, C.; Zhao, R.; He, X.; Yang, P.; Shi, B.; You, X.; Jiang, Z. Weakly Humidity-Dependent Proton-Conducting COF Membranes. *Adv. Mater.* **2020**, *32*, No. 2005565.
- (37) Guo, Z.-C.; Shi, Z.-Q.; Wang, X.-Y.; Li, Z.-F.; Li, G. Proton Conductive Covalent Organic Frameworks. *Coord. Chem. Rev.* **2020**, *422*, No. 213465.
- (38) He, X.; Yang, Y.; Wu, H.; He, G.; Xu, Z.; Kong, Y.; Cao, L.; Shi, B.; Zhang, Z.; Tongsh, C.; Jiao, K.; Zhu, K.; Jiang, Z. De Novo Design of Covalent Organic Framework Membranes toward Ultrafast Anion Transport. *Adv. Mater.* **2020**, *32*, No. 2001284.
- (39) Tao, S.; Zhai, L.; Dinga Wonanke, A. D.; Addicoat, M. A.; Jiang, Q.; Jiang, D. Confining H₃PO₄ Network in Covalent Organic Frameworks Enables Proton Super Flow. *Nat. Commun.* **2020**, *11*, No. 1981.
- (40) Wu, X.; Hong, Y.-l.; Xu, B.; Nishiyama, Y.; Jiang, W.; Zhu, J.; Zhang, G.; Kitagawa, S.; Horike, S. Perfluoroalkyl-Functionalized Covalent Organic Frameworks with Superhydrophobicity for Anhydrous Proton Conduction. *J. Am. Chem. Soc.* **2020**, *142*, 14357–14364.
- (41) Yang, Y.; He, X.; Zhang, P.; Andaloussi, Y. H.; Zhang, H.; Jiang, Z.; Chen, Y.; Ma, S.; Cheng, P.; Zhang, Z. Combined Intrinsic and Extrinsic Proton Conduction in Robust Covalent Organic Frameworks for Hydrogen Fuel Cell Applications. *Angew. Chem., Int. Ed.* **2020**, *59*, 3678–3684.


- (42) Wang, S.; Wang, Q.; Shao, P.; Han, Y.; Gao, X.; Ma, L.; Yuan, S.; Ma, X.; Zhou, J.; Feng, X.; Wang, B. Exfoliation of Covalent Organic Frameworks into Few-Layer Redox-Active Nanosheets as Cathode Materials for Lithium-Ion Batteries. *J. Am. Chem. Soc.* **2017**, *139*, 4258–4261.
- (43) Li, J.; Jing, X.; Li, Q.; Li, S.; Gao, X.; Feng, X.; Wang, B. Bulk COFs and COF Nanosheets for Electrochemical Energy Storage and Conversion. *Chem. Soc. Rev.* **2020**, *49*, 3565–3604.
- (44) Li, W.; Yang, C.-X.; Yan, X.-P. A Versatile Covalent Organic Framework-Based Platform for Sensing Biomolecules. *Chem. Commun.* **2017**, *53*, 11469–11471.
- (45) Singh, H.; Tomer, V. K.; Jena, N.; Bala, I.; Sharma, N.; Nepak, D.; De Sarkar, A.; Kailasam, K.; Pal, S. K. A Porous, Crystalline Truxene-Based Covalent Organic Framework and Its Application in Humidity Sensing. *J. Mater. Chem. A* **2017**, *5*, 21820–21827.
- (46) Zhou, Z.; Zhong, W.; Cui, K.; Zhuang, Z.; Li, L.; Li, L.; Bi, J.; Yu, Y. A Covalent Organic Framework Bearing Thioether Pendant Arms for Selective Detection and Recovery of Au from Ultra-Low Concentration Aqueous Solution. *Chem. Commun.* **2018**, *54*, 9977–9980.
- (47) Zhou, T.-Y.; Xu, S.-Q.; Wen, Q.; Pang, Z.-F.; Zhao, X. One-Step Construction of Two Different Kinds of Pores in a 2D Covalent Organic Framework. *J. Am. Chem. Soc.* **2014**, *136*, 15885–15888.
- (48) Guan, X.; Li, H.; Ma, Y.; Xue, M.; Fang, Q.; Yan, Y.; Valtchev, V.; Qiu, S. Chemically Stable Polyarylether-Based Covalent Organic Frameworks. *Nat. Chem.* **2019**, *11*, 587–594.
- (49) Guo, Z.; Zhang, Y.; Dong, Y.; Li, J.; Li, S.; Shao, P.; Feng, X.; Wang, B. Fast Ion Transport Pathway Provided by Polyethylene Glycol Confined in Covalent Organic Frameworks. *J. Am. Chem. Soc.* **2019**, *141*, 1923–1927.
- (50) Zhao, S.; Jiang, C.; Fan, J.; Hong, S.; Mei, P.; Yao, R.; Liu, Y.; Zhang, S.; Li, H.; Zhang, H.; Sun, C.; Guo, Z.; Shao, P.; Zhu, Y.; Zhang, J.; Guo, L.; Ma, Y.; Zhang, J.; Feng, X.; Wang, F.; Wu, H.; Wang, B. Hydrophilicity Gradient in Covalent Organic Frameworks for Membrane Distillation. *Nat. Mater.* **2021**, *20*, 1551–1558.
- (51) Zhu, Y.; Shao, P.; Hu, L.; Sun, C.; Li, J.; Feng, X.; Wang, B. Construction of Interlayer Conjugated Links in 2D Covalent Organic Frameworks Via Topological Polymerization. *J. Am. Chem. Soc.* **2021**, *143*, 7897–7902.
- (52) Deng, H.; Grunder, S.; Cordova, K. E.; Valente, C.; Furukawa, H.; Hmadeh, M.; Gandara, F.; Whalley, A. C.; Liu, Z.; Asahina, S.; Kazumori, H.; O’Keeffe, M.; Terasaki, O.; Stoddart, J. F.; Yaghi, O. M. Large-Pore Apertures in a Series of Metal-Organic Frameworks. *Science* **2012**, *336*, 1018–1023.
- (53) Li, H.; Ding, J.; Guan, X.; Chen, F.; Li, C.; Zhu, L.; Xue, M.; Yuan, D.; Valtchev, V.; Yan, Y.; Qiu, S.; Fang, Q. Three-Dimensional Large-Pore Covalent Organic Framework with Stp Topology. *J. Am. Chem. Soc.* **2020**, *142*, 13334–13338.
- (54) Chen, X.; Geng, K.; Liu, R.; Tan, K. T.; Gong, Y.; Li, Z.; Tao, S.; Jiang, Q.; Jiang, D. Covalent Organic Frameworks: Chemical Approaches to Designer Structures and Built-in Functions. *Angew. Chem., Int. Ed.* **2020**, *59*, 5050–5091.
- (55) Yu, S.-B.; Lyu, H.; Tian, J.; Wang, H.; Zhang, D.-W.; Liu, Y.; Li, Z.-T. A Polycationic Covalent Organic Framework: A Robust Adsorbent for Anionic Dye Pollutants. *Polym. Chem.* **2016**, *7*, 3392–3397.
- (56) Xu, T.; An, S.; Peng, C.; Hu, J.; Liu, H. Construction of Large-Pore Crystalline Covalent Organic Framework as High-Performance Adsorbent for Rhodamine B Dye Removal. *Ind. Eng. Chem. Res.* **2020**, *59*, 8315–8322.
- (57) Kuhn, P.; Thomas, A.; Antonietti, M. Toward Tailorable Porous Organic Polymer Networks: A High-Temperature Dynamic Polymerization Scheme Based on Aromatic Nitriles. *Macromolecules* **2009**, *42*, 319–326.
- (58) Xu, Y.; Jin, S.; Xu, H.; Nagai, A.; Jiang, D. Conjugated Microporous Polymers: Design, Synthesis and Application. *Chem. Soc. Rev.* **2013**, *42*, 8012–8031.
- (59) Thommes, M.; Kaneko, K.; Neimark, A. V.; Olivier, J. P.; Rodriguez-Reinoso, F.; Rouquerol, J.; Sing, K. S. W. Physisorption of Gases, with Special Reference to the Evaluation of Surface Area and Pore Size Distribution (Iupac Technical Report). *Pure Appl. Chem.* **2015**, *87*, 1051–1069.
- (60) Chen, Q.; Dwyer, C.; Sheng, G.; Zhu, C.; Li, X.; Zheng, C.; Zhu, Y. Imaging Beam-Sensitive Materials by Electron Microscopy. *Adv. Mater.* **2020**, *32*, No. 1907619.
- (61) Gong, X.; Gnanasekaran, K.; Chen, Z.; Robison, L.; Wasson, M. C.; Bentz, K. C.; Cohen, S. M.; Farha, O. K.; Gianneschi, N. C. Insights into the Structure and Dynamics of Metal-Organic Frameworks Via Transmission Electron Microscopy. *J. Am. Chem. Soc.* **2020**, *142*, 17224–17235.
- (62) Zuluaga, S.; Fuentes-Fernandez, E. M. A.; Tan, K.; Xu, F.; Li, J.; Chabal, Y. J.; Thonhauser, T. Understanding and Controlling Water Stability of MOF-74. *J. Mater. Chem. A* **2016**, *4*, 5176–5183.
- (63) Abad-Zapatero, C.; Erickson, J. W. Protein Data Bank. <https://www.rcsb.org/structure/3PEP/> (accessed Sept 01, 2021).
- (64) Hodgman, M. J.; Garrard, A. R. A Review of Acetaminophen Poisoning. *Crit. Care Clin.* **2012**, *28*, 499–516.
- (65) Sun, Q.; Fu, C.-W.; Aguila, B.; Perman, J.; Wang, S.; Huang, H.-Y.; Xiao, F.-S.; Ma, S. Pore Environment Control and Enhanced Performance of Enzymes Infiltrated in Covalent Organic Frameworks. *J. Am. Chem. Soc.* **2018**, *140*, 984–992.




JACS Au
AN OPEN ACCESS JOURNAL OF THE AMERICAN CHEMICAL SOCIETY



Editor-in-Chief
Prof. Christopher W. Jones
Georgia Institute of Technology, USA

Open for Submissions 

pubs.acs.org/jacsau  ACS Publications
Most Trusted. Most Cited. Most Read.